

Rotational evolution of the Crab pulsar in the wind braking model

F. F. Kou and H. Tong

Xinjiang Astronomical Observatory, Chinese Academy of Sciences, Urumqi, Xinjiang 830011, China; tonghao@xao.ac.cn

2015.3 v3

ABSTRACT

The pulsar wind model is updated by considering the effect of particle density and pulsar death. It can describe both the short term and long term rotational evolution of pulsars consistently. It is applied to model the rotational evolution of the Crab pulsar. The pulsar is spun down by a combination of magnetic dipole radiation and particle wind. The parameters of the Crab pulsar, including magnetic field, inclination angle, and particle density are calculated. The primary particle density in acceleration region is about 10^3 times the Goldreich-Julian charge density. The lower braking index between glitches is due to a larger outflowing particle density. This may be glitch induced magnetospheric activities in normal pulsars. Evolution of braking index and the Crab pulsar in $P - \dot{P}$ diagram are calculated. The Crab pulsar will evolve from magnetic dipole radiation dominated case towards particle wind dominated case. Considering the effect of pulsar “death”, the Crab pulsar (and other normal pulsars) will not evolve to the cluster of magnetars but downwards to the death valley. Different acceleration models are also considered. Applications to other sources are also discussed, including pulsars with braking index measured, and the magnetar population.

Key words: pulsars: general – pulsars: individual (PSR B0531+21) – stars: magnetar – stars: neutron – wind

1 INTRODUCTION

The Crab pulsar (PSR B0531+21) is a young radio pulsar with a spin frequency $\nu = 30.2$ Hz and frequency derivative $\dot{\nu} = -3.86 \times 10^{-10}$ Hz/s (Lyne et al. 1993). Its characteristic magnetic field is about 7.6×10^{12} G at the magnetic poles¹. The Crab pulsar has been monitored continuously for decades years by various telescopes since it was discovered in 1968 (Lyne et al. 1993; Lyne et al. 2015; Wang et al. 2012). Its braking index is $n = 2.51 \pm 0.01$ (Lyne et al. 1993). Different braking index values 2.45, 2.57 and 2.3 are also reported between glitches (Wang et al. 2012; Lyne et al. 2015). Observational details are given in Table 1.

Long-term observations have found that almost all pulsars (except accreting X-ray pulsars in binary systems) are spinning down. The spin-down behavior can be described by a power law (Lyne et al. 1993):

$$\dot{\nu} = -k\nu^n, \quad (1)$$

here, k is usually taken as a constant and n is the brak-

ing index. The braking index and second braking index are defined respectively (Livingstone et al. 2005):

$$n = \frac{\nu\ddot{\nu}}{\dot{\nu}^2}, \quad (2)$$

$$m = \frac{\nu^2\ddot{\nu}}{\dot{\nu}^3}, \quad (3)$$

where ν is the pulsar spin frequency, $\dot{\nu}$, $\ddot{\nu}$ and $\ddot{\nu}$ are the first, second and third frequency derivative, respectively. The spinning down of pulsars is usually assumed to be braked by the magnetic dipole radiation (Shapiro & Teukolsky 1983). In the magnetic dipole radiation model, a neutron star rotates uniformly in vacuo at a frequency ν and possesses a magnetic moment μ . The corresponding slowdown rate is:

$$\dot{\nu} = -\frac{8\pi^2\mu^2}{3Ic^3}\nu^3\sin^2\alpha, \quad (4)$$

where $\mu = 1/2BR^3$ is the magnetic dipole moment (B is the polar magnetic field and R is the radius of neutron star), $I = 10^{45}$ g · cm² is the moment of inertia, c is the speed of light, and α is the angle between the rotational axis and the magnetic axis (i.e., the inclination angle). The spin down behavior of pulsar in this model can be described as $\dot{\nu} \propto \nu^3$. The braking index is exactly three if μ , I , and α are

¹ Assuming all the rotational energy loss is due to magnetic dipole radiation in vacuum, $B_c = 6.4 \times 10^{19} \sqrt{P\dot{P}}$ G

constant. To date, only eight pulsars, including the Crab pulsar, have measured the meaningful braking indices for they are young and own relatively larger $\dot{\nu}$ (Espinoza et al. 2011; Lyne et al. 2015). Their braking indices are all smaller than three. It means that there are other physical processes needed to slow down the pulsar.

Many mechanisms have been proposed in order to explain the braking index observations, e.g., the pulsar wind model (Xu & Qiao 2001; Wu et al. 2003; Contopoulos & Spitkovsky 2006; Yue et al. 2007), a changing magnetic field strength (Lin et al. 2004; Chen & Li 2006; Espinoza et al. 2011), a changing inclination angle (Lyne et al. 2013), and additional torques due to accretion (Liu et al. 2014). However, these models are more or less not consistent with observations or can not simulate the long-term evolution of pulsars. And these models can not explain the different braking indices detected between glitches (Wang et al. 2012; Lyne et al. 2015). Furthermore, the effect of pulsar death (death line, Ruderman & Sutherland 1975; or death valley, Chen & Ruderman 1993; Zhang et al. 2000) should be considered in modeling the long term rotational evolution of the pulsar (Contopoulos & Spitkovsky 2006).

The pulsar wind model considers both the pulsar spin-down and the particle acceleration in the magnetosphere (Xu & Qiao 2001; Wu et al. 2003). In this paper, an updated pulsar wind model is built based on previous researches (Xu & Qiao 2001; Yue et al. 2007; Contopoulos & Spitkovsky 2006; Li et al. 2012). It includes: (1) Both magnetic dipole radiation and particle outflow, and their dependence on the inclination angle; (2) The particle outflow depends on the specific acceleration model; (3) The primary particle density may be much larger than the Goldreich-Julian charge density; (4) The effect of pulsar death is considered in modeling the rotational evolution of the pulsar. This model can calculate both the short term and long term evolution of pulsars. It is applied to the Crab pulsar which has the most detailed timing observations. Possible applications to other sources are also illustrated.

The pulsar wind model and model calculations of the Crab pulsar are presented in section 2. Discussions and conclusions are given in section 3 and section 4, respectively.

2 SPIN-DOWN OF THE CRAB PULSAR IN THE PULSAR WIND MODEL

2.1 Description of the pulsar wind model

In the pulsar wind model, the rotational energy is consumed by magnetic dipole radiation and particle acceleration (Xu & Qiao 2001). The magnetic dipole radiation is related to the perpendicular component of the magnetic moment ($\mu_{\perp} = \mu \sin \alpha$), the power of magnetic dipole radiation is (Shapiro & Teukolsky 1983):

$$\dot{E}_d = \frac{2\mu^2\Omega^4}{3c^3} \sin^2 \alpha, \quad (5)$$

where $\Omega = 2\pi\nu$ is the angular speed of the pulsar. The effect of parallel component of magnetic moment ($\mu_{\parallel} = \mu \cos \alpha$) is responsible for particles acceleration (Ruderman & Sutherland 1975). Acceleration gaps are formed above the polar gap, primary particles are generated and accelerated in these gaps. The energy taken away by these particles dependents

Table 1. Observations of the Crab pulsar.

Pulsar parameter	Values
Epoch(MJD)	40000.0
ν (Hz)	30.225437 ^a
$\dot{\nu}$ (10 ⁻¹⁰ Hz/s)	-3.86228 ^a
$\ddot{\nu}$ (10 ⁻²⁰ Hz/s ²)	1.2426 ^a
$\ddot{\nu}$ (10 ⁻³⁰ Hz/s ³)	-0.64 ^a
Braking index n	2.51 \pm 0.01 ^a
Second braking index m	10.15 ^a
Inclination angle α ($^{\circ}$)	(45 \sim 70) ^b
Age	915 yr (from 1054 to 1969)

Notes: (a): Observed spin frequency and its derivatives are parameters in the Taylor expansion

$\nu = \nu_0 + \dot{\nu}_0(t - t_0) + \frac{1}{2}\ddot{\nu}_0(t - t_0)^2 + \frac{1}{6}\ddot{\nu}_0(t - t_0)^3$ for 1969 \sim 1975 (Lyne et al. 1993). For there are rare glitches occurred in this interval. Later observations (Lyne et al. 2015) confirm previous results.

(b):The range of inclination angle is given by modeling the pulse profile of the Crab pulsar (Dyks et al. 2003; Harding et al. 2008; Watter et al. 2009; Du et al. 2012; Lyne et al. 2013).

on the acceleration potential drop. The corresponding rotational energy loss rate is (Xu & Qiao 2001):

$$\dot{E}_p = 2\pi r_p^2 c \rho_e \Delta\phi, \quad (6)$$

where $r_p = R(R\Omega/c)^{1/2}$ is polar gap radius, $\rho_e = \kappa\rho_{GJ}$ is the primary particle density ($\rho_{GJ} = \Omega B/(2\pi c)$ is the Goldreich-Julian charge density, Goldreich & Julian 1969), $\Delta\phi$ is the corresponding acceleration potential of the acceleration region, and κ is a coefficient related to primary particle density which can be constrained by observations². The maximum acceleration potential for a rotating dipole is $\Delta\Phi = \mu\Omega^2/c^2$ (Ruderman & Sutherland 1975). Then equation (6) can be rewritten as (considering that the particle acceleration is mainly related to the parallel component of magnetic moment):

$$\dot{E}_p = \frac{2\mu^2\Omega^4}{3c^3} 3\kappa \frac{\Delta\phi}{\Delta\Phi} \cos^2 \alpha. \quad (7)$$

The magnetic dipole radiation and the outflow of particle wind may contribute independently. Then the total rotational energy loss rate is:

$$\begin{aligned} \dot{E} &= \dot{E}_d + \dot{E}_p = \frac{2\mu^2\Omega^4}{3c^3} (\sin^2 \alpha + 3\kappa \frac{\Delta\phi}{\Delta\Phi} \cos^2 \alpha) \\ &= \frac{2\mu^2\Omega^4}{3c^3} \eta, \end{aligned} \quad (8)$$

where $\eta = \sin^2 \alpha + 3\kappa\Delta\phi/\Delta\Phi \cos^2 \alpha$. The first and second items of expression η are respectively for magnetic dipole and particle wind. If the acceleration potential $\Delta\phi = 0$, there are no particles accelerated in the gap, the pulsar is just braked down by the magnetic dipole radiation. The acceleration potential is model dependent (Xu & Qiao 2001; Wu et al. 2003). A particle density of κ times Goldreich-Julian

² Primary particle density in the acceleration gap is: $\rho_e = |e|[n_+ + n_-]$, but Goldreich-Julian ‘‘charge’’ density is: $\rho_{GJ} = |e|[n_+ - n_-]$ (Yue et al. 2007). It is reasonable to infer that: $\kappa \geq 1$.

charge density is considered. Expressions of η are given in Table 2 for various acceleration models³. The rotational evolution of the pulsar can be written as:

$$-I\Omega\dot{\Omega} = \frac{2\mu^2\Omega^4}{3c^3}\eta, \quad (9)$$

According equation (2) and (3), the braking index and second braking index in the wind braking model are:

$$n = 3 + \frac{\Omega}{\eta} \frac{d\eta}{d\Omega}, \quad (10)$$

$$m = 15 + 12 \frac{\Omega}{\eta} \frac{d\eta}{d\Omega} + \left(\frac{\Omega}{\eta} \frac{d\eta}{d\Omega}\right)^2 + \frac{\Omega^2}{\eta} \frac{d^2\eta}{d\Omega^2}. \quad (11)$$

Equation (9), (10) and (11) are all functions of magnetic field B , inclination angle α and particle density κ (Ω and its derivatives are observational inputs, see Table 1).

Taking these expressions of η (Table 2) back to equation (9), it can be seen that: as the pulsar spinning down (Ω decreases), the effect of particle wind becomes stronger. If there are particles flowing out, it means that there are still particle acceleration in magnetosphere (the pulsar is still active). However, as pulsar spinning down, the potential drop may not sustain the need to accelerate particles (Ruderman & Sutherland 1975). Besides, observations do not support pulsars to evolve unceasingly in these pulsar wind models (Young et al. 1999; Contopoulos & Spitkovsky 2006). Therefore, ‘‘pulsar death’’ must be considered in modeling the long term rotational evolution of the pulsar. As the spin angular speed decreasing to the death value, the radio emission tends to stop. And when pulsar is death, the pulsar is braked only by magnetic dipole radiation. Here, the VG(CR) model is employed to show the effect of pulsar death by introducing a piecewise function deduction (details are shown in the appendix A).

$$\eta_{\text{VG}}^{\text{CR}} = \begin{cases} \sin^2 \alpha + 4.96 \times 10^2 \kappa \left(1 - \frac{\Omega_{\text{death}}}{\Omega}\right) B_{12}^{-8/7} \Omega^{-15/7} \cos^2 \alpha, & \text{if } \Omega > \Omega_{\text{death}} \\ \sin^2 \alpha, & \text{if } \Omega < \Omega_{\text{death}}. \end{cases} \quad (12)$$

The death period is defined as $\Omega_{\text{death}} = 2\pi/P_{\text{death}}$ (Contopoulos & Spitkovsky 2006; Tong & Xu 2012):

$$P_{\text{death}} = 2.8 \left(\frac{B}{10^{12} \text{ G}}\right)^{1/2} \left(\frac{V_{\text{gap}}}{10^{12} \text{ V}}\right)^{-1/2} \text{ s}. \quad (13)$$

V_{gap} can be viewed as the maximum acceleration potential drop in the open field line regions and $V_{\text{gap}} = 10^{13} \text{ V}$ is chosen in the following calculations (Contopoulos & Spitkovsky 2006). It is introduced according to Contopoulos & Spitkovsky (2006) (see also later works by Li et al. 2012). In this way, the effect of pulsar death can be incorporated in the rotational energy loss rate. The effect of pulsar death is discussed in more detail in section 2.5. For young pulsars ($\Omega \gg \Omega_{\text{death}}$), the effect of pulsar death is negligible. But for the long-term evolution of pulsars, especially when the period approaches the death period, the effect of pulsar death is significant.

³ As shown in Table 2, the models of VG(CR) and SCLF(I) are very similar with each other. Crab parameters calculated in these two models are also similar (shown later).

Table 2. The Expressions of η for nine particle acceleration models.

No.	Acceleration model	η
1	VG (CR)	$\sin^2 \alpha + 4.96 \times 10^2 \kappa B_{12}^{-8/7} \Omega^{-15/7} \cos^2 \alpha$
2	VG (ICS)	$\sin^2 \alpha + 1.02 \times 10^5 \kappa B_{12}^{-22/7} \Omega^{-13/7} \cos^2 \alpha$
3	SCLF (II,CR)	$\sin^2 \alpha + 38 \kappa B_{12}^{-1} \Omega^{-7/4} \cos^2 \alpha$
4	SCLF (II, ICS)	$\sin^2 \alpha + 2.3 \kappa B_{12}^{-22/13} \Omega^{-8/13} \cos^2 \alpha$
5	SCLF (I)	$\sin^2 \alpha + 9.8 \times 10^2 \kappa B_{12}^{-8/7} \Omega^{-15/7} \cos^2 \alpha$
6	OG	$\sin^2 \alpha + 2.25 \times 10^5 \kappa B_{12}^{-12/7} \Omega^{-26/7} \cos^2 \alpha$
7	CAP	$\sin^2 \alpha + 54 \kappa B_{12}^{-1} \Omega^{-2} \cos^2 \alpha$
8	NTVG (CR)	$\sin^2 \alpha + 13.7 \beta^{0.14} \kappa B_{12}^{-1} \Omega^{-1.76} \cos^2 \alpha$
9	NTVG (ICS)	$\sin^2 \alpha + 69.6 \gamma^{-1} \kappa B_{12}^{-1} \Omega^{-1.88} \cos^2 \alpha$

Notes: Particle density $\rho_e = \kappa \rho_{\text{G,J}}$ is taken in all these models. B_{12} is the magnetic field strength in units of 10^{12} G .

(a): The models 1 ~ 5 are based on the pulsar wind model of Xu & Qiao (2001). The VG and SCLF are respectively the acceleration models: vacuum gap and space charge limit flow. In the vacuum gap (Ruderman & Sutherland 1975), curvature radiation (CR) and inverse Compton scattering (ICS) are considered (Zhang et al. 2000). In the SCLF case, regimes II and I are defined by field saturated or not (Arons & Scharlemann 1979; Harding & Muslimov 1998). Three models are introduced: CR for SCLF model in regime II, ICS for SCLF model in regime II, and the SCLF model in regime I.

(b): The OG means the outer gap, is self-sustaining and limited by the electron-positron pair produced by collisions between high-energy photons (Zhang & Cheng 1997). The modification by Wu et al. (2003) is adopted. (c): The CAP model is a phenomenological model of constant potential $\Delta\phi = 3 \times 10^{12} \text{ V}$ (Yue et al. 2007).

(d): The NTVG shorts for near threshold vacuum gap. In this model, the electron-positron pair produced at or near the kinematic threshold $\hbar\omega = 2mc^2 / \sin\theta$ because of superstrong surface magnetic field (Gil & Melikidze 2002). $\beta = 52$ is taken in the CR case, and $\gamma = 14$ is taken in the ICS case (Abrahams & Shapiro 1991; Wu et al. 2003).

2.2 Understanding the braking index of the Crab pulsar

Parameters of the Crab pulsar are calculated in this section. The VG(CR) model is taken as an example to show the calculation process. For pulsars with the observed ν , $\dot{\nu}$, $\ddot{\nu}$ and $\ddot{\nu}$, their observational braking index n and second braking index m can be get by equation (2) and (3). Pulsar parameters such as magnetic field, inclination angle, and particle density can be calculated by these three equations (9), (10) and (11). The primary particle density may be $10^3 \sim 10^4$ times of Goldreich-Julian charge density (Yue et al 2007). According the observational range of inclination angle and the characteristic magnetic field (which can be viewed as order of magnitude estimation of the true magnetic field), the range of particle density κ can be limited by equation (9) and (10). In our calculation, $\kappa = 10^3$ is adopted⁴, the inclination angle α and magnetic field B are about 55° and $8.1 \times 10^{12} \text{ G}$ which are consistent with observational constraints. The second braking index calculated by equation (11) is 10.96, which is roughly consistent with the observed value 10.15 (Lyne et al. 1993), considering the observational uncertainties (Lyne et al. 1993, 2015).

The magnetic field and inclination angle are assumed to be constant in the pulsar wind model. The particle density decreases in long-term evolution of pulsars but remains unchanged in short duration at early time. Figure 1 shows the braking index of the Crab pulsar as a function of spin

⁴ We should note that the κ is related to the primary particles in the acceleration gap but not the total out-flow particles.

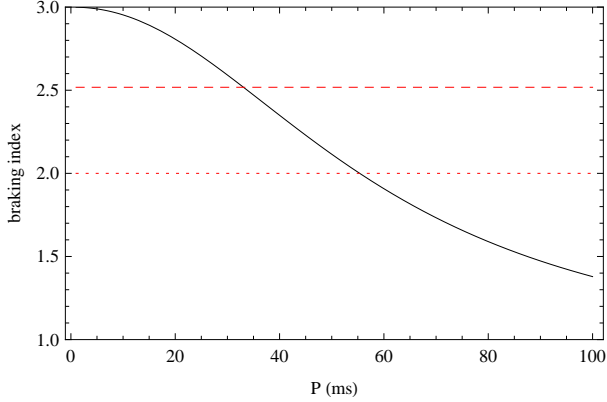


Figure 1. The braking index of the Crab pulsar as function of spin period in the VG(CR) model. The dashed line is observational braking index of 2.51. The dotted line is braking index in the transition point ($n = 2$).

Table 3. Parameters of the Crab pulsar calculated in various acceleration models.

Models	κ 10^3	α $^\circ$	B_{12}	P_0 ms	P_t ms	P_d s	T_t 10^3 yr	T_d 10^5 yr
VG(CR)	1	55	8.1	18.8	55	2.52	2.77	0.78
VG(ICS)	0.1	60	7.5	18.9	63	2.58	3.50	1.67
SCLF(II CR)	2	58	7.5	18.9	68	2.59	3.93	2.24
SCLF(II ICS)	0.6	44	5.0	19.2	—	3.16	—	30.1
SCLF(I)	0.6	57	7.8	18.8	55	2.45	2.77	0.78
OG	20	59	8.2	18.5	42	2.47	1.63	0.07
CAP	3	52	8.3	18.9	58	2.46	3.08	1.14
NTVG(CR)	3	57	7.7	19.5	67	2.56	4.10	2.52
NTVG(ICS)	30	54	7.5	19.4	62	2.58	3.58	1.81

Notes:

- (a): κ is the coefficient of primary particle density $\rho_e = \kappa \rho_{GJ}$.
 (b): α and B_{12} are respectively the inclination angle and the magnetic field.
 (c): P_0 is the initial period.
 (d): P_t and T_t are the transition period and corresponding age. At this transition point the braking index is 2. Because the minimum braking index of model SCLF(ICS) is 2.4, there is no such a transition point, which can be seen in the evolution in $P - \dot{P}$ diagram (see Figure 7).
 (e): P_d and T_d are the period and age when pulsar stops radio emission. The death period is calculated by equation (13).

period. As the pulsar period increases, the braking index decreases from 3 to 1. It illustrates that the Crab pulsar is initially braked by magnetic dipole ($n \rightarrow 3$) and then by the particle wind ($n \rightarrow 1$). We take $n = 2$ as the transition point (see Figure 5, at $n = 2$, the slop of the curve is 0) and the corresponding spin period is about 55 ms. Since Table 1 has shown the timing observations of the Crab pulsar in 1969 (its age is 915 years old by then), its initial period is $P_0 \approx 18.8$ ms in AD 1054 by integrating equation (9). The calculations of all acceleration models are shown in Table 3. As shown in this table, the particle densities are different in different models, but are all more than 100 times of ρ_{GJ} . The inclination angles is within the observational range. The initial periods are all about 19 ms.

2.3 An increasing particle density results in a lower braking index during glitches

A braking index 2.3 has been monitored after the removal of the effects of glitches during an epoch when there are many glitches occurred (Lyne et al. 2015). It is different from the long term underlying braking index 2.51 of the Crab pulsar. Previously, Wang et al. (2012) have measured two different values of braking index $n = 2.45$ and $n = 2.57$ between glitches. They attribute it to the effect of varying particle wind strength (Wang et al. 2012). It is generally accepted that glitch is caused by the inner effect but may lead to some effect in the outer magnetosphere⁵, for example: the changing of primary particle density during this epoch. In the pulsar wind model, it can be denoted by the changing coefficient of particle density $\kappa = \kappa(t)$. Then equation (10) should be modified:

$$n = 3 + \frac{\Omega}{\eta} \frac{d\eta}{d\Omega} + \frac{\kappa}{\eta} \frac{d\eta}{d\kappa} \frac{\Omega}{\dot{\kappa}} \frac{\dot{\kappa}}{\kappa}. \quad (14)$$

Equation (14) can be rewritten as:

$$n = 3 + \frac{\Omega}{\eta} \frac{d\eta}{d\Omega} - \frac{\kappa}{\eta} \frac{d\eta}{d\kappa} \frac{\tau_c}{\tau_\kappa}, \quad (15)$$

where $\tau_c = -\frac{\Omega}{2\dot{\Omega}}$ is the characteristic age, $\tau_\kappa = \frac{\kappa}{2\dot{\kappa}}$ can be viewed as the typical time scale of the changing particle density. When the magnetosphere is in equilibrium (i.e., when the glitch activities of the pulsar is not very active), the time scale of particle density variation (τ_κ) may be very large (i.e., larger than the characteristic age τ_c). The third term in equation (15) does not contribute. But, if they are comparable with each other, the braking index changes substantially. In other words, when the outflow particle density increases and the effect of particle wind becomes stronger, means $\tau_\kappa > 0$ or $\dot{\kappa} > 0$, the braking index will be smaller than 2.51. But when the outflow particle density decreases ($\tau_\kappa < 0$ or $\dot{\kappa} < 0$), the braking index will be larger than 2.51. As the out-flow particle density tending to a certain value (larger or smaller than previous value), the braking index tends to its underlying value (2.51). Generally, the increased (or decreased) component of the outflow particle density (may be 0.1%) is so much small that it can be ignored.

Figure 2 shows the braking index as function of τ_κ for the Crab pulsar in the VG(CR) model. In order to better understand the observations of $n < 2.51$ (Lyne et al. 2015), we consider the $\tau_\kappa > 0$ only. As we can see in this figure, the braking index is insensitive to τ_κ when it is larger than 10^4 yr. But, when it is comparable with the characteristic age (about 10^3 yr), the braking index decreases sharply. When braking index is 2.3, the changing rate of the particle density is $\dot{\kappa} \approx 1.2 \times 10^{-8} \text{ s}^{-1}$. In this interval (from MJD 51000 to MJD 53000, about 5 years), the particle density has changed by $2 \rho_{GJ}$. The change of particle density will result in changes of radiation energy loss rate and period derivative. Their changes respectively are: $\delta \dot{E} \approx 2 \times 10^{35} \text{ erg/s}$ and $\delta \dot{P} \approx 1.88 \times 10^{-16} \text{ s/s}$.

⁵ Glitch induced magnetospheric activities are very common in the case of magnetars (Dib & Kaspi 2014).

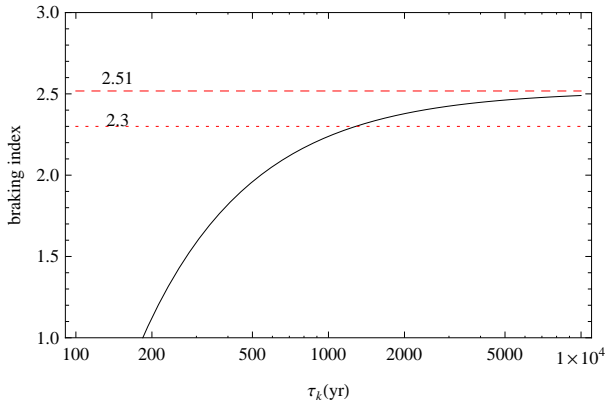


Figure 2. The braking index of the Crab pulsar as function of τ_κ in the VG(CR) model. The dashed line is the underlying braking index 2.51. The dotted line is the smaller braking index 2.3 measured during glitch activities (Lyne et al. 2015, Figure 7 there).

The pulsar wind model can be tested with observations (Jodrell Bank monthly ephemeris of the Crab pulsar⁶). The effect of glitches is not taken into consideration in the pulsar wind model. The changes of period and period derivative caused by glitches should be added (Lyne et al. 2015). Figure 3 is the model calculation compared with observations (without modelling the transient variation caused by glitches). When the amplitude of glitches is relatively small, the change of particle density is not obvious, then the model calculations (the blue points) fit well with observations (the black points). However, when the amplitude of glitches is large, the effect of glitches must be added (the red points). Moreover, the effect of particle density change should be taken into consideration. A factor $\delta\dot{P} = 1.88 \times 10^{-16}$ s/s (which is calculated above) is added to the red points (from MJD 51804.75 afterwards), shown as the green points. The green points can match the general trend of the observations.

2.4 Long term evolution of the Crab pulsar

The pulsar period and its first derivative evolution with time in the VG(CR) model are shown in the first and second panel of Figure 4. The curves evolve slowly in its early age and then rise sharply, indicating that the Crab pulsar is mainly braked by magnetic dipole radiation firstly and then mainly by particle wind. The transition period is 55 ms and age of the Crab pulsar will be 2771 calculated in the VG(CR) model (see Table 3). The braking index evolution with time in the VG(CR) model is shown in the third panel of Figure 4. Braking index decreases from 3 to $6/7$ –different minimum braking indices for different acceleration models. The bottom panel of Figure 4 shows the second braking index evolution with time. The curve gradually decreases from 15 to $30/49$. Figure 5 shows the evolution of the Crab pulsar in $P - \dot{P}$ diagram from birth to its 30000 years old. These points are respectively taken when the Crab pulsar is: 1, 915, 2771, 9000 and 30000 years old. Period derivative

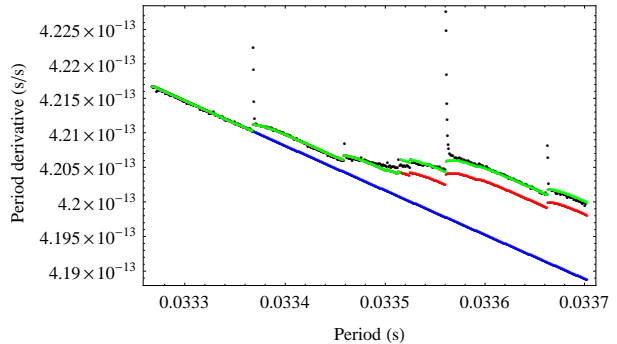


Figure 3. Evolution of the Crab pulsar in $P - \dot{P}$ diagram in VG(CR) model compared with observations. The black points are timing results from Jodrell Bank monthly ephemeris. The blue points are the rotational evolution of Crab pulsar in the VG(CR) model. The red ones are obtained by adding the effect of glitches (Lyne et al. 2015, Table 3 there). And the green ones are the summation of red points and a factor $\delta\dot{P} \approx 1.88 \times 10^{-16}$ s/s (from MJD 51804.75 afterwards), which may be caused by the change of out-flow particle density. At first, the black, blue, red, and green points are coincide with each other. (Notes: The fitting does not model the transient process caused by glitches.)

evolves with period by a function of $\dot{P} \propto P^{2-n}$ (Espinoza et al. 2011). In the log-log plot, the evolution curve evolves with a slope $(2-n)$. As the braking index falling from 3 to 1, the pulsar evolve from magnetic dipole radiation dominated case (the left points) to the particle wind dominated case (the right points) and the bottom is the transition point ($n = 2$). Clearly, the curve evolves more sharply after the transition point. The asymptotic behaviors are discussed in the appendix B.

2.5 The effect of pulsar death

As shown in the Figure 5, the line evolves up right with a slope about 1 after the transition point just like PSR J1734-3333 whose braking index is 0.9 ± 0.2 (Espinoza et al. 2011). If the pulsar continually evolve in this trend, it would not dead and might end itself as a magnetar. It will be hard to explain the observations for: (1) The number of magnetars are smaller than radio pulsars and most of the pulsars occupy the central region in the $P - \dot{P}$ diagram (see Figure 6); (2) Only a small portion of magnetars are radio emitters (Olausen & Kaspi 2014); (3) The properties of the Crab pulsar, PSR J1734-3333 and other high magnetic field pulsars are significantly different from magnetars (Ng & Kaspi 2011). As pulsars slow-down, the density of outflow particles may decrease and the effect of particle wind will recede (for the SCLF cases, the number of particles (or κ) may close to constant, but the particle density still decreases because a reducing Goldreich-Julian charge density). Therefore, the effect of pulsar death must be included in modeling the long-term rotational evolution of pulsars.

The essential condition of radio emission for a pulsar is its pair production (Sturrock 1971; Ruderman & Sutherland 1975). The so called pulsar “death” means the stopping of pulsar emission (Ruderman & Sutherland 1975; Chen & Ruderman 1993; Zhang et al. 2000; Contopoulos & Spitkovsky 2006). The death defined by Ruderman & Sutherland (1975)

⁶ <http://www.jb.man.ac.uk/pulsar/crab.html>, data from 1982 February 15 (MJD 45015) to 2014 October 15 (MJD 56945) are used here.

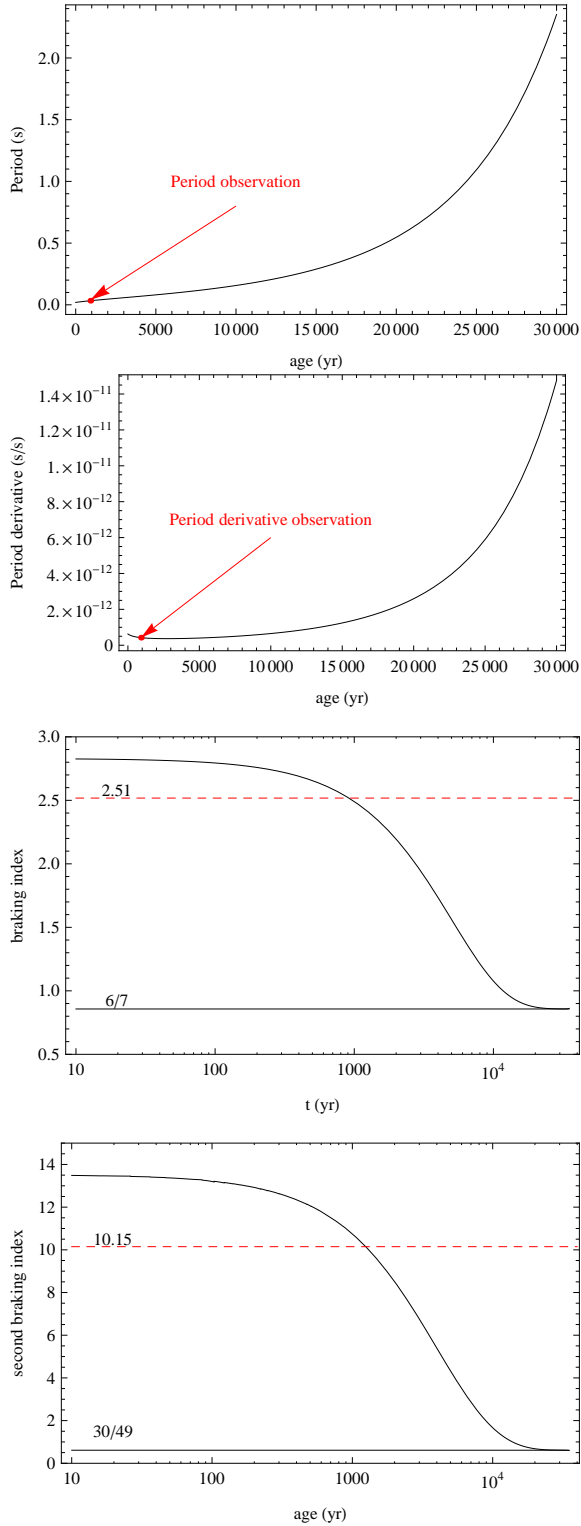


Figure 4. Rotational evolution of the Crab pulsar from birth to 30 thousands years in the VG(CR) model. The first and second panels are respectively the period and period derivative evolution with time. The points are observations of period and its derivative (Lyne et al. 1993). The third and fourth panels are respectively the braking index and second braking index evolution with time. The dashed lines are observed values and the solid lines are respectively the minimum braking index and second braking index in the VG(CR) model.

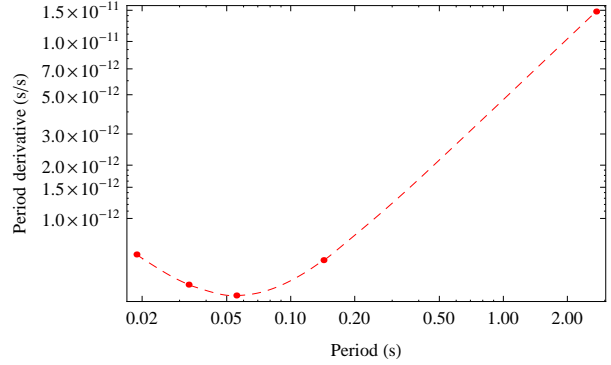


Figure 5. Evolution of the Crab pulsar in the $P-\dot{P}$ diagram. Five points are chosen when the pulsar is: 1, 915, 2771, 9000 and 30000 years old.

is that: a pulsar dead when the maximum potential drop $\Delta\Phi$ available from the pulsar is smaller than the acceleration potential needed to accelerate particles. Because this death line is model dependent, Chen & Ruderman (1993) proposed death “valley” by modifying the boundary conditions. And this death “valley” was updated by considering different particle acceleration and photon radiation processes (Zhang et al. 2000). However these works are just to separate pulsars with radio emission from those without. Contopoulos & Spitkovsky (2006) included the effect of pulsar death when modeling the rotational evolution of pulsars. However, the braking indices there are always larger than three. Considering particle acceleration and pulsar death simultaneously may give a comprehensive interpretation for both short and long-term rotational evolution of pulsars.

The visual explanation for pulsar death in the pulsar wind model is that the particles in the magnetosphere are exhausted and there are no primary particles generated. For the physical understanding, we can refer to the equation (8), expressions $\Delta\Phi \propto \Omega^2$ and $\Delta\phi$ (i.e., $\Delta\phi_{\text{VGCR}} = 2.8 \times 10^{13} R_6^{2/7} B_{12}^{-1/7} \Omega^{-1/7}$ V, Xu & Qiao 2001), with the pulsar spinning down, the maximum potential of the pulsar ($\Delta\Phi$) drops, when the maximum potential can not meet the need to accelerate particles ($\Delta\phi > \Delta\Phi$), the pulsar death. Besides, the acceleration potential is weakly dependent on the Ω , that is why we can make calculations under the constant acceleration potential (the CAP model) (Yue et al. 2007). Figure 6 shows the long-term evolutions of the Crab pulsar in the VG(CR) model. The dashed curve is the line shown in Figure 5 and the solid is the one with pulsar death (according to equation (12)). These two lines evolve similar at the early age, and divide obviously after the transition point. The second line falls down afterwards and moves down-right with a slop about -1 finally. The initial period and transition period can be calculated according the second line, which are same with the values given by the first line within precision. Indicating that the effect of pulsar death can be ignored in the early time. As mentioned before, the particle density decreases as pulsar spin-down. The gap between these two lines is caused by the reducing of particle density. When the spin period of Crab approaches to the death period 2.52s, the radio emission tends to stop and the slop of the second line is very large. Crab evolution in

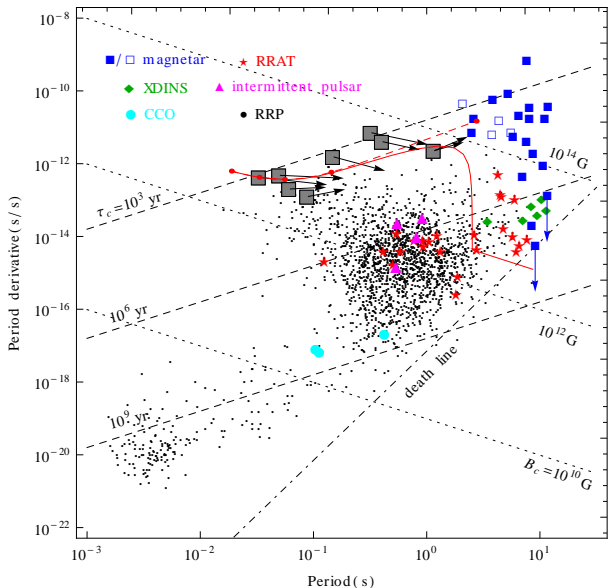


Figure 6. Rotational evolution of the Crab pulsar in the VG(CR) model. The dashed curve is the evolution without considering pulsar death. The solid line is the one considering pulsar death. The $P - \dot{P}$ diagram has listed all known radio pulsars, magnetars, and millisecond pulsars (updated from Figure 1 in Tong & Wang 2014). The dot-dashed line represents the fiducial death line (Ruderman & Sutherland 1975). Pulsars with meaningful braking indices (Espinoza et al. 2011; Lyne et al. 2015) are defined by large square. The arrows represent their evolution directions and each arrow indicate its motion in the next 10000 yr (For the Vela pulsar, 20000 yr is used; 5000 yr for PSR J1846-0258 and PSR J1119-6127).

various acceleration models are given in Figure 7. The bottom line is the evolution curve in SCLF(ICS) model. There is no transition point, indicating that the particle wind effect of this model is very weak. The top line is the evolution of the Crab pulsar in the OG model. This model is for high-energy radiation, the death of this model may differ from radio emission models. The results here for the OG model are just crude approximations to show the effect of pulsar death. Evolution of the Crab pulsar in other models are similar with each other.

3 DISCUSSIONS

In the magnetic dipole radiation model, a pulsar is assumed as a magnetic dipole rotating in vacuum. It is just a low-order approximation of the true magnetosphere, and there must be particles acceleration and generation process so that the radio emission can be received. The actual magnetosphere surrounding the pulsar must be filled with plasma and corotate with pulsar because of magnetic freeze. According the special relativity, the corotation magnetosphere can not infinitely extend but only exist within the light cylinder. The magnetosphere is divided into two parts by the light cylinder: the closed magnetic field lines and the open magnetic field lines (including polar gap and outer gap). In the open field line region, particles are accelerated, generate radiation and flow out (thus taken away some of the rotational energy of the central neutron star). In the pulsar

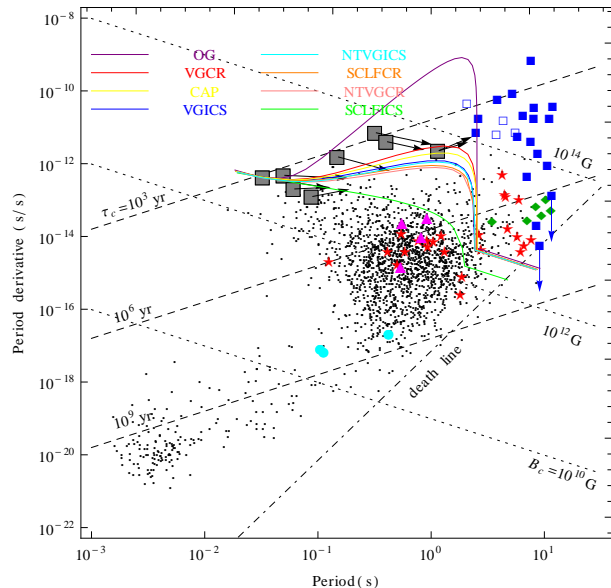


Figure 7. Rotational evolution of the Crab pulsar in all acceleration models. Because the VG(CR) model and SCLF(I) model are very similar, their lines are coincident. Only the line in the VG(CR) model is plotted. See also Figure 6 for explanations.

wind model, the pulsar is braked down by magnetic dipole radiation and particle wind. But in the electric current loss model, the electric current flow generates a spin-down torque (Harding et al. 1999; Beskin et al. 2007). Based on the same magnetospheric physics, the pulsar wind model and the current loss case are just different point of views, will produce the same results (e.g. Section 3.2 in Tong et al. 2013). And they can be used to check each other. It is meaningful to take advantage of the existing information and explain more observations. The particle wind worked on pulsar spin-down was first proven by observations of intermittent pulsar PSR B1931+24 whose radio emission switches between “on” and “of” state (Kramer et al. 2006). Corresponding calculations for intermittent pulsars in pulsar wind model were made by Li et al. (2014).

As one of the best observed pulsar, observations of the Crab pulsar are relatively comprehensive (see Table 1 & timing results from Jodrell Bank website). It will be the best target to test radiation models. The pulsar parameters can be calculated by equations (9), (10) and (11) when model dependent acceleration potential (or η) is given (see Table 2). The Goldreich-Julian charge density is taken as the primary particle density in these models of Xu & Qiao (2001) and Wu et al (2003). However, Yue et al. (2007) constrained the primary particle density by observations of several pulsars and predicted that it should be $10^3 \sim 10^4$ times of Goldreich-Julian charge density. In our calculations, the primary particle density is at least 100 times of Goldreich-Julian charge density. In the VG(CR) model, a particle density $10^3 |\rho_{GJ}|$ is chosen. When applying the pulsar wind model to intermittent pulsars, a Goldreich-Julian charge density is assumed (Li et al. 2014). As the pulsar spin-down, its out-flow particle density decreases. In the $P - \dot{P}$ diagram, these intermittent pulsars are on the right of those young pulsars (see Figure 6). This may explain the different particle density in the Crab pulsar and intermittent pulsars.

Other studies also found the need for a high particle density in the pulsar magnetosphere, e.g., when modeling the eclipse of the double pulsar system, giant pulses of the Crab pulsar, and magnetar X-ray spectra (Lyutikov 2008 and references therein), optical/ultraviolet excess of X-ray dim isolated neutron stars (Tong et al. 2010, 2011). Magnetohydrodynamical simulations of the Crab nebula also require a much higher electron flow from the magnetosphere (Buhler & Blandford 2014 and references therein). Besides, a super Goldreich-Julian current has been proposed in a series theoretical works about the pairs creations in the acceleration gap (Timokhin & Arons, 2013; Zanotti et al. 2012; Hirotani 2006). Combined with the results in this paper, it is possible that there are high density plasmas (e.g., 10^3 - 10^4 times the Goldreich-Julian density) in both open and closed field line regions in the pulsar magnetosphere.

3.1 Applications to other sources

Here the updated pulsar wind model is employed to compare with the observations of the Crab pulsar. It can also be applied to other sources. For eight pulsars with meaningful braking index measured (Espinoza et al. 2011; Lyne et al. 2015), their magnetospheric parameters can also be calculated, including magnetic field, inclination angle, particle density etc. But the higher second frequency derivatives of some pulsars (Hobbs et al. 2010) may be attributed to the fluctuation of magnetosphere (Contopoulos 2007). During this process, more information will be helpful to constrain the model parameters, e.g., inclination angle, second braking index. Their evolution on the $P - \dot{P}$ diagram can be calculated, which will be similar to Figure 6. The pulsar PSR J1734-3333 has braking index $n = 0.9 \pm 0.2$ (Espinoza et al. 2011). Its rotational energy loss rate will be dominated by the particle wind. Also from Figure 6, the braking indices of young pulsars will naturally be divided into two groups. Braking indices of pulsars in the first group are close to three, their evolution directions are down to the right in the $P - \dot{P}$ diagram ($\dot{P} \propto P^{2-n} \sim P^{-1}$). Braking indices in the second group are close to one and their evolution directions are up to the right ($\dot{P} \propto P^{2-n} \sim P^1$). Generally speaking, sources in the second group will be older than the ones in the first group. At present, there are some hints for the evolution of pulsar braking index (Espinoza 2013). Future more observations will deepen our understanding on this aspect.

Glitch is a phenomenon of the pulsar suddenly spinning up and then slowing down by a larger rate. In the pulsar wind model, the lower braking index 2.3 during glitches (of the Crab pulsar) is due to the larger out-flow particle density. The increasing particle density is a possible performance associated with glitches. Glitches induced magnetospheric activities are very common in magnetars (Kaspi et al. 2003; Dib & Kaspi 2014). For the high magnetic field pulsar PSR J1846-0258, it also shows a smaller braking index after glitch (Livingstone et al. 2011). The cause of a smaller braking index may be similar to the Crab pulsar case. Due to a larger particle outflow, the pulsar should experience some net spindown after glitch. This has already been observed (Livingstone et al. 2010). Some primary calculations for PSR J1846-0258 has been done previously (Tong 2014, based on a wind braking model designed for magnetars). The smaller

braking index of PSR J1846-0258 after glitch is consistent with the results here.

From Figure 6 and Figure 7, the pulsar will go up-right in the $P - \dot{P}$ diagram in the wind braking dominated case. Therefore, for pulsars in the up right corner of the $P - \dot{P}$ diagram (e.g., high magnetic field pulsars and magnetars), their true dipole magnetic field may be much lower than the characteristic magnetic field. For magnetar SGR 1806-20, its characteristic magnetic field is about 5×10^{15} G (Tong et al. 2013). This dipole magnetic field is too high to understand comfortably (Vigano et al. 2013). Using the physical braking mechanism in this paper, the dipole magnetic field of SGR 1806-20 will be much lower. In the late stage of a pulsar, it will bent and go downward in the $P - \dot{P}$ diagram. The Crab pulsar and other pulsars will not evolve into the cluster of magnetars. Furthermore, for magnetars, they also will go downward in the $P - \dot{P}$ diagram when they are aged enough. This may corresponds to the case of low magnetic field magnetars (Tong & Xu 2012).

4 CONCLUSIONS

An updated pulsar wind model which considered the effect of particle density and pulsar death is developed. It is employed to calculate parameters and simulate the evolution of the Crab pulsar. The braking index $n < 3$ is the combined effect of magnetic dipole radiation and particle wind. The lower braking indices measured between glitches are caused by the increasing particle density. By adding the glitch parameters and a change of period derivative caused by the change of particle density, the theoretical evolution curve is well fitted with observations (Figure 3). This may be viewed as glitch induced magnetospheric activities in normal pulsars. Giving the model dependent acceleration potential drop, the magnetic field, inclination angle and particle density of the Crab pulsar can be calculated. The evolution of braking index and the Crab pulsar in $P - \dot{P}$ diagram can be obtained. In the $P - \dot{P}$ diagram, the Crab pulsar will evolve towards the death valley, not to the cluster of magnetars (Figure 6). Different acceleration models are also considered. The possible application of the present model to other sources (pulsars with braking index measured, and the magnetar population) is also mentioned.

ACKNOWLEDGMENTS

The authors would like to thank the Referee Barsukov D.P. for helpful comments and R.X.Xu, J.B.Wang for discussions. H.Tong is supported Xinjiang Bairen project, West Light Foundation of CAS (LHXZ201201), Qing Cu Hui of CAS, and 973 Program (2015CB857100).

APPENDIX A: CONSIDERATION OF PULSAR "DEATH"

The treatment of Contopoulos & Spitkovsky (2006) is employed in the following. Assuming that the open field line

regions rotate at a angular velocity Ω_{open} but not the angular velocity of the neutron star⁷.

$$\Omega_{\text{open}} = \Omega - \Omega_{\text{death}} \quad (\text{A1})$$

The particle density in this acceleration gap is κ times the Goldreich-Julian charge density:

$$\rho_e \approx \kappa \frac{\Omega_{\text{open}} B}{2\pi c}, \quad (\text{A2})$$

The energy taken away by the out-flowing particles is:

$$\dot{E}_p = 2\pi r_p^2 c \rho_e \Delta\phi. \quad (\text{A3})$$

The perpendicular component and parallel component of the magnetic moment are respectively related to the magnetic dipole radiation and particle acceleration. The rotation energy loss rate can be written as:

$$\begin{aligned} \dot{E} &= \dot{E}_d + \dot{E}_p = \frac{2\mu^2 \Omega^4}{3c^3} (\sin^2 \alpha + 3\kappa(1 - \frac{\Omega_{\text{death}}}{\Omega}) \frac{\Delta\phi}{\Delta\Phi} \cos^2 \alpha) \\ &= \frac{2\mu^2 \Omega^4}{3c^3} \eta, \end{aligned} \quad (\text{A4})$$

with the expression of η

$$\eta = \sin^2 \alpha + 3\kappa(1 - \frac{\Omega_{\text{death}}}{\Omega}) \frac{\Delta\phi}{\Delta\Phi} \cos^2 \alpha. \quad (\text{A5})$$

For a constant acceleration potential $\Delta\phi = 3 \times 10^{12} \text{V}$, correspondingly,

$$\eta = \sin^2 \alpha + 54\kappa(1 - \frac{\Omega_{\text{death}}}{\Omega}) R_6^3 B_{12}^{-1} \Omega^{-2} \cos^2 \alpha. \quad (\text{A6})$$

For the physical acceleration models, η is model dependent. Its expression in the VG(CR) case is calculated in the following. The potential drop of open field lines is (Ruderman & Sutherland 1975):

$$\Delta\phi = \frac{\Omega_{\text{open}} B}{c} h^2, \quad (\text{A7})$$

where Ω_{open} is the angular frequency of the open field lines (Contopoulos & Spitkovsky 2006), h is the thickness of the gap, $h = 1.1 \times 10^4 \rho_6^{2/7} \Omega_{\text{open}}^{-3/7} B_{12}^{-4/7} \text{cm}$ and $\rho = 2.3 \times 10^8 R_6^{1/2} \Omega_{\text{open}}^{-1/2} \text{cm}$ is the curvature radius of the open field lines ($\rho_6 = \rho/10^6 \text{cm}$) (Ruderman & Sutherland 1975). The expression of η can be rewritten as:

$$\begin{aligned} \eta &= \sin^2 \alpha + 4.96 \times 10^2 \kappa \\ &\times (1 - \frac{\Omega_{\text{death}}}{\Omega})^{6/7} R_6^{-19/7} B_{12}^{-8/7} \Omega^{-15/7} \cos^2 \alpha \end{aligned} \quad (\text{A8})$$

The exponent of $(1 - \frac{\Omega_{\text{death}}}{\Omega})$ is the minimum braking index in the VG(CR) model, $n = 6/7$ (Li et al. 2014). In the wind braking model, the minimum braking index is always around one (Li et al. 2014). Therefore, it is taken as one in equation (12) (for all the acceleration models). During the numerical calculations, the neutron star radius is taken as 10^6cm (i.e., $R_6 = 1$).

APPENDIX B: ASYMPTOTIC BEHAVIORS IN FIGURE 4 AND 5

In the pulsar wind model, the pulsar is braked down by the combination of magnetic dipole radiation and particle wind. The effect of particle wind is more and more important with pulsar spinning down. As shown in Figure 4, the period and period derivative evolve up sharply with age. If the pulsar braking is dominated by magnetic dipole radiation, equation (1) can be written as:

$$\dot{\nu} = -k\nu^3. \quad (\text{B1})$$

the evolution of spin frequency is $\nu = (2kt)^{-1/2}$ (assuming initial spin frequency is very large). Correspondingly, the period and period derivative evolution with time are respectively: $P = (2kt)^{1/2}$, and $\dot{P} = k(2kt)^{-1/2}$. If the pulsar is braked down mainly by particle wind, the braking index is about 1. The spin-down power law is :

$$\dot{\nu} = -k\nu. \quad (\text{B2})$$

the evolution of spin frequency is $\nu \propto \exp(-kt)$. Correspondingly, the period and period derivative evolution with time are respectively: $P \propto \exp(kt)$, and $\dot{P} \propto \exp(kt)$. Clearly, the period and period derivative evolve faster by the exponential form.

REFERENCES

- Abrahams A. M., Shapiro S. L., 1991, ApJ, 374, 652
 Arons J., Scharlemann E. T., 1979, ApJ, 231, 854
 Beskin V.S., Nokhrina E. E., 2007, Ap & SS, 308, 569
 Buhler R., Blanford R., 2014, RPPH, 77, 6901
 Chen K., Ruderman M. A., 1993, ApJ, 402, 264
 Chen W. C., Li X. D., 2006, A&A, 450, L1
 Contopoulos I., Spitkovsky A., 2006, ApJ, 643, 1139.
 Contopoulos I. 2007, A&A, 475,639
 Dib R., Kaspi V. M., 2014, ApJ, 784, 37
 Du Y. J., Qiao G. J., Wang W., 2012, ApJ, 748, 84
 Dyks J., Rudak B., 2003, ApJ, 598, 1201
 Espinoza C. M., Lyne A. G., Kramer M., et al., 2011, ApJ, 741, L13
 Espinoza C. M., 2013, IAUS, 291, 195
 Gil J., Melikidze G. I., 2002, ApJ, 577, 909
 Goldreich P., Julian W. H., 1969, ApJ, 157, 869
 Harding A. K., Muslimov A. G., 1998, ApJ, 508, 328
 Harding, A. K., Contopoulos, I., Kazanas, D., 1999, ApJ, 525, 125
 Harding A. K., Stern J. V., Dyks J., et al., 2008, ApJ, 680, 1378
 Hirotani K., 2006, ApJ V., 652, 1475
 Hobbs G., Lyne A. G., Kramer M., 2010, MNRAS, 402, 1027
 Kaspi V. M., Gavriil F. P., Woods P. M., 2003, ApJ, 588, L93
 Kramer M., Lyne A. G., O'Brien J. T., et al., 2006, Science, 312, 549
 Li J., Spitkovsky A., Tchekhovskoy A., 2012, ApJ, 746, 60
 Li L., Tong H., Yan W. M., et al., 2014, ApJ, 788, 16
 Lin J. R., Zhang S. N., 2004, ApJ, 615, L133
 Liu X. W., Xu R. X., Qiao G. J., et al., 2014, RAA, 14, 85
 Livingstone M. A., Kaspi V. M., Gavriil F. P., et al., 2005, ApJ, 619, 1046

⁷ In fact, particles in the acceleration gap rotate with a angular speed between the spinning speed of pulsar surface and the open field lines (Ruderman & Sutherland 1975). We use the angular speed of the open field lines as the boundary condition to describe the pulsar death because the acceleration potential is insensitive to it in this pulsar wind model.

- Livingstone M. A., Kaspi V. M., Gavriil F. P., 2010, *ApJ*, 710, 1710
- Livingstone M. A., Kaspi V. M., Ng C. Y., et al., 2011, *ApJ*, 730, 66
- Lyne A. G., Pritchard R. S., Smith F. G., 1993, *MNRAS*, 265, 1003
- Lyne A. G., Smith F. G., Weltevrede P., et al., 2013, *Science*, 342, 589
- Lyne A. G., Jordan C. A., Smith F.G., et al., 2015, *MNRAS*, 446, 857
- Lyutikov M., 2008, *AIP Conference Proceedings*, 968, 77
- Ng C. Y., Kaspi V. M., 2011, *AIP Conference Proceedings*, 1379, 60
- Olausen S. A., Kaspi V. M., 2014, *ApJS*, 212, 6
- Ruderman M. A., Sutherland P. G., 1975, *ApJ*, 196, 51
- Shapiro S. L., Teukolsky S. A., 1983, *Black holes, white dwarfs, and neutron stars*, John Wiley & Sons, New York
- Sturrock P. A., 1971, *ApJ*, 164, 529
- Timokhin A. N., Arons J., 2013, *MNRAS* V., 429, p.20
- Tong H., Xu R. X., Peng Q. H., et al., 2010, *RAA*, 10, 553
- Tong H., Xu R. X., Song L. M., 2011, *RAA*, 11, 1371
- Tong H., Xu R. X., 2012, *ApJ*, 757, L10
- Tong H., Xu R. X., Song L. M., et al., 2013, *ApJ*, 768, 144
- Tong H., 2014, *ApJ*, 784, 86
- Tong H., Wang W., 2014, *arXiv:1406.6458*
- Vigano D., Rea N., Pons J. A., et al., 2013, *MNRAS*, 434, 123
- Wang J., Wang N., Tong H., et al., 2012, *Astrophys.Space Sci.*, 340, 307
- Watters K. P., Romani R. W., Weltevrede P., et al., 2009, *ApJ*, 695, 1289
- Wu F., Xu R. X., Gil J., 2003, *A&A*, 409, 641
- Xu R. X., Qiao G. J., 2001, *ApJ*, 561, L85
- Yue Y. L., Xu R. X., Zhu W. W., 2007, *Advance in Space Research*, 40, 1491
- Young M. D., Manchester R. N., Johnston S., 1999, *Nature*, 400, 848
- Zanotti O., Morozova V., Ahmedov B., 2012, *A & A V.*, 540, A126
- Zhang L., Cheng K. S., 1997, *ApJ*, 487, 370
- Zhang B., Harding A. K., Muslimov A. G., 2000, *ApJ*, 531, L135